

The Power of Characterizing Pore-Fluid Distribution for Microscopic CO₂ Injection Studies in Tight Sandstones

Alkharraa, Hamad; Wolf, Karl-Heinz; AlQuraishi, Abdulrahman; Mahmoud, Mohamed; AlDuhailan, Mohammed; Zitha, Pacelli

DOI

[10.3390/min13070895](https://doi.org/10.3390/min13070895)

Publication date

2023

Document Version

Final published version

Published in

Minerals

Citation (APA)

Alkharraa, H., Wolf, K.-H., AlQuraishi, A., Mahmoud, M., AlDuhailan, M., & Zitha, P. (2023). The Power of Characterizing Pore-Fluid Distribution for Microscopic CO₂ Injection Studies in Tight Sandstones. *Minerals*, 13(7), Article 895. <https://doi.org/10.3390/min13070895>

Important note

To cite this publication, please use the final published version (if applicable).
Please check the document version above.

Copyright


Other than for strictly personal use, it is not permitted to download, forward or distribute the text or part of it, without the consent of the author(s) and/or copyright holder(s), unless the work is under an open content license such as Creative Commons.

Takedown policy

Please contact us and provide details if you believe this document breaches copyrights.
We will remove access to the work immediately and investigate your claim.

Article

The Power of Characterizing Pore-Fluid Distribution for Microscopic CO₂ Injection Studies in Tight Sandstones

Hamad AlKharraa^{1,*}, Karl-Heinz Wolf¹, Abdulrahman AlQuraishi², Mohamed Mahmoud³ , Mohammed AlDuhailan⁴ and Pacelli Zitha^{1,*}

¹ Department of Geotechnology, Delft University of Technology, Stevinweg 1, 2628 CN Delft, The Netherlands; k.h.a.a.wolf@tudelft.nl

² National Centre for Oil & Gas Technology, King Abdulaziz City for Science and Technology, Riyadh 12354, Saudi Arabia

³ College of Petroleum Engineering and Geosciences, King Fahd University of Petroleum & Minerals, Dhahran 34464, Saudi Arabia

⁴ Saudi Aramco, Dhahran 31311, Saudi Arabia

* Correspondence: h.s.h.alkharraa@tudelft.nl (H.A.); p.l.j.zitha@tudelft.nl (P.Z.)

Abstract: The microscopic structure of low-permeability tight reservoirs is complicated due to diagenetic processes that impact the pore-fluid distribution and hydraulic properties of tight rocks. As part of an ongoing study of carbon dioxide-enhanced oil and gas recovery (CO₂-EOR/EGR) and CO₂ sequestration, this research article adopts an integrated approach to investigate the contribution of the micropore system in pore-fluid distribution in tight sandstones. A new dimensionless number, termed the microscopic confinement index (MCI), was established to select the right candidate for microscopic CO₂ injection in tight formations. Storativity and containment indices were essential for MCI estimation. A set of experiments, including routine core analysis, X-ray diffraction (XRD), scanning electron microscopy (SEM), mercury injection capillary pressure (MICP), and nuclear magnetic resonance (NMR), was performed on three tight sandstone rock samples, namely Bandera, Kentucky, and Scioto. Results indicate that the presence of fibrous illite acting as pore bridging in Bandera and Kentucky sandstone samples reduced the micropore-throat proportion (MTMR), leading to a significant drop in the micropore system confinement in Kentucky and Bandera sandstone samples of 1.03 and 0.56, respectively. Pore-filling kaolinite booklets reduced the micropore storativity index (MSI) to 0.48 in Kentucky and 0.38 in Bandera. On the other hand, the absence of fibrous illite and kaolinite booklets in Scioto sandstone led to the highest micropore system capability of 1.44 MTMR and 0.5 MSI to store and confine fluids. Therefore, Scioto sandstone is the best candidate for CO₂ injection and storage among the tested samples of 0.72 MCI.

Keywords: microscopic gas confinement; micropore system's storativity; pore-fluid distribution; clay minerals; CO₂ injection and storage; low-permeability micropore system



Citation: AlKharraa, H.; Wolf, K.-H.; AlQuraishi, A.; Mahmoud, M.; AlDuhailan, M.; Zitha, P. The Power of Characterizing Pore-Fluid Distribution for Microscopic CO₂ Injection Studies in Tight Sandstones. *Minerals* **2023**, *13*, 895. <https://doi.org/10.3390/min13070895>

Academic Editors: Barbara Cantucci and Giordano Montegrossi

Received: 28 April 2023

Revised: 13 June 2023

Accepted: 25 June 2023

Published: 30 June 2023



Copyright: © 2023 by the authors. Licensee MDPI, Basel, Switzerland. This article is an open access article distributed under the terms and conditions of the Creative Commons Attribution (CC BY) license (<https://creativecommons.org/licenses/by/4.0/>).

1. Introduction

Tight formations have received significant interest as unconventional reservoirs due to the substantial proliferation of worldwide resources exhibiting these attributes [1–3]. Tight reservoirs are classified based on their porosity and permeability, displaying threshold values of less than 10% and 0.1 mD, respectively [4–6]. Some studies extend the range of permeability to less than 1 mD [2,7]. Tight reservoirs are also defined as those structures characterized by low permeability, either close to or distant from the source rocks, that require the use of hydraulic fracturing to enhance hydrocarbon production [8–10]. Tight sandstone is an essential type of unconventional resource [11] and is characterized by complex pore systems due to its depositional conditions [12,13]. Tight sandstones can be classified using the reservoir quality index (RQI), and any reservoir with RQI within the range of 0 to 0.5 microns is considered tight; however, complex pore structures (throats and

bodies) can render the RQI inconclusive in tight sandstone characterization [14,15]. Table 1 shows the typical tight formation properties gathered from the literature.

Table 1. Typical rock/formation and fluid properties of tight oil reservoirs.

Property	Typical Range	References
Permeability	<2 mD	[2,7]
Porosity	<20%	[15]
Pore-throat size	0.03 μm –2 μm	[16,17]
Clay content	7%–30%	[18]
Lithology	shale, sandstone, carbonate	[19]
Driving mechanism	poor connectivity	[20]

Industry professionals and researchers express varying opinions on the permeability threshold for tight reservoirs. While some designate the value of 0.1 mD, others prefer different cut-off values [2,7,15]. In tight reservoirs, the permeability cut-off value can vary due to the pore system's heterogeneity [16]. We therefore believe that pore-size characterization is essential in the classification of these reservoirs. Pore-fluid distribution (PFD) is complex in tight reservoirs due to the rock's depositional and diagenetic conditions [19,20]. PFD, including the bound volume index (BVI) and free fluid index (FFI), significantly influences fluid flow behavior in sandstone rocks [20–22]. Hence, understanding these indices and their controlling factors is vital for the successful injection of fluid(s), such as CO₂ injection, which has gained a lot of momentum recently for many reasons including carbon geo-sequestration (CGS) from an environmental perspective and enhanced oil recovery (CO₂-EOR) [23,24]. The CO₂-EOR technique has proved to have substantial potential in increasing oil recovery in conventional and tight reservoirs [25]. Injecting CO₂ into oil reservoirs can be performed under miscible or immiscible conditions. However, numerous studies indicate that oil recovery is higher when CO₂ is injected in a miscible state or as a supercritical fluid. When the injection pressure exceeds the minimum miscibility pressure (MMP), the CO₂ and oil phases become miscible, resulting in no interfacial tension between them. This leads to oil swelling and reduced oil viscosity, which ultimately increases oil recovery [26–28].

There are several primary factors involved in the control of sandstone pore distribution, including mineralogy, diagenetic processes, grain size, and pore structure [29–31]. It is noteworthy that primary pores and micropores are the principal components of the pore-fluid distribution in sandstones [32]. Primary pores are voids between detrital grains that form during the depositional process, while micropores originate prior to the depositional process and commonly exist between detrital grains and authigenic clay minerals [33–35]. Sandstone rocks exhibit a proportional relationship between the primary pore and grain size [35–37].

Compaction primarily reduces primary pores and thus decreases sandstone's total porosity [38]. Several studies claim that common long-side, concavo-convex, sutured grain contacts correspond to considerable rock compaction, decreasing primary pores [39,40]. The results of the investigation into the effect of grain shape on porosity by Beard and Weyl in 1973 [41] show that as the sphericity increases, the primary pores decrease because of the tight packing. Furthermore, sorting accounts for the variety in sandstone grain size and correlates well with porosity [42]. Sandstones with good sorting attributes possess a significant number of primary pores due to grain size homogeneity [43,44]. However, poor sorting leads to complex pore-throat size distribution, leading to a sharp reduction in porosity due to small particles filling the intergranular pores [45–47]. The dissolution of feldspar can cause a remarkable increase in the percentage of primary pores [48], leading to better pore connectivity [49].

The presence of clay minerals can reduce or enhance pore-size distribution in sandstone rocks. Several studies have investigated the impact of total clay content on the petrophysical properties of tight sandstone [50–52]. Yuan et al. [53] indicate the existence of

an inverse relationship between both porosity and permeability with clay content. Kaolinite booklets can fill the rock pores and hence lower sandstone's porosity [54,55]; however, kaolinite has fewer effects on permeability [55]. Conversely, the presence of fibrous illite clay tends to clog the pore–throat diameter and consequently leads to reduced permeability [56]. Quartz overgrowth affects porosity and permeability by including a reduction in the reducing primary pores in sandstones [57–59]. However, a clay coating can preserve primary pores by coating the detrital quartz grains, thus inhibiting their overgrowth [60,61].

Chima et al. [42] studied the impact of pore structure on NMR T_2 distributions at various pore sizes. The authors found that sandstone samples with a higher percentage of primary pores exhibit longer NMR T_2 peak values, suggesting the existence of a direct relation between movable water and primary pores. This further implies that a higher movable fluid proportion corresponds to more interconnected pores [62,63]. Both movable and bound-fluid volumes can be determined using both centrifuge and NMR measurements [64–66]. In these methods, movable fluid is discharged from interconnected pores using a high-speed centrifuge, while bound fluid is confined inside the micropore system due to the clay presence and capillarity [66,67]. Notably, the presence of clay minerals reduces primary pores, turning them into micropores [68,69]. Micropore systems are characterized by having pore bodies smaller than 10 microns and micropore throats smaller than 1 micron in size [70]. These systems play significant roles in EOR, CO_2 sequestration, and hydrogen storage [71–73].

Previous studies have focused on movable fluid and other dominant factors affecting fluid flow in tight sandstones. Nevertheless, a limited number of studies have investigated the relationship between the proportion of the micropore system and factors that influence gas and fluid confinement. This study explores the relationship between tight sandstone's micropore system and pore-fluid distribution. In order to achieve this goal, we develop an integrated workflow of set of experimental measurements on different sets of tight outcrop sandstone samples. New dimensionless indices are developed in order to provide novel selection criteria for planning CO_2 injection and optimal storage processes.

2. Materials and Methods

A suite of three tight sandstones was received from Kocurek Industries companyTM, Caldwell, TX, USA (Figure 1). The samples comprised Bandera, Kentucky, and Scioto sandstones cut from several U.S outcrops. These outcrops are not representative of any hydrocarbon reservoir, and their samples are typically used in petroleum engineering laboratories for research purposes. In preparation for the experimental work, cylindrical samples, 3.8 cm in diameter and 7.6 cm in length, were dried and vacuumed for two days at 75 °C. Figure 2 is a flow chart showing the methodology used to satisfy the goal of this study. The upper parts of these dry core plugs were cut into 1 cm thick disks in order to subject them to X-ray diffraction (XRD) and scanning electron microscopy (SEM) analyses. XRD was performed on ground samples to determine the mineral composition of sandstone samples using a RigakuTM ULTIMA IV powder X-Ray diffractometer instrument with $Cu\alpha$ radiation at 40 kV and 40 mA (Figure 2a) from Osaka, Japan. The measurements were acquired at a 2θ range from 3° to 100°, with a step increment of 0.02° and a duration of 8 min. XRD patterns were then analyzed using X'Pert High Score Software (Malvern, UK). Thin disks of circa 0.5 cm were used for SEM experiments. We utilized a TESCANTM instrument, from Brno, the Czech Republic instrument, (model MIRA3) coupled with an EDX detector to generate SEM density images with a nanometric pixel resolution. This allowed us to identify the micropore and clay morphologies of these sandstones (Figure 2b) [74,75]. We then conducted porosity and permeability measurements at ambient conditions. A VinciTM helium porosimeter from Nanterre, France was then used in order to determine the samples' total connected porosity, while a Core-LabTM from Houston, TX, USA, gas permeameter was utilized for the assessment of gas permeability and Klinkenberg liquid permeability (Figure 2c). A synthetic formation brine with a salinity of 236.84 ppm was used in this study to represent connate water saturation. The brine was prepared using NaCl, $CaCl_2$,

MgCl₂, Na₂SO₄, and NaHCO₃, dissolved in deionized water (Figure 2d). The brine density and viscosity were measured using a benchtop density meter (Anton Paar-DMA 4500 M) and an Oswald viscometer, respectively. Subsequently, these dry sandstone samples were saturated with synthetic brine, utilizing a saturation unit at room temperature and with a pressure of 13.8 MPa (2000 psi) for 24 h to ensure full brine saturation (Figure 2e). NMR measurements were performed on brine-saturated sandstones to determine the relaxation time (T_2) using the Oxford Instruments 2 MHz GeoSpec 2–75 equipped with Green Imaging Technologies (v6.1) software (Figure 2f). NMR T_2 measurements were generated using the Carr–Purcell–Meiboom–Gill (CPMG) pulse sequence, which is proportional to the pore-size distribution of sandstones [76–78]. The main acquisition parameters used in these experiments are listed in Table 2.



Figure 1. Outcrop sandstone samples used in this study.

Subsequently, we utilized a URC-628 CoreTest™ centrifuge from California, USA to analyze brine-saturated core samples at a rotational speed of 4000 revolutions per minute (rpm) (Figure 2g), using air as the displacing phase. NMR T_2 measurements were then conducted on these partially saturated core samples to assess the bound-fluid volume trapped in the micropores (Figure 2h), and hence to determine pore-fluid distributions. The BVI was determined as the cumulative NMR porosity after the centrifuge test in order to indicate the fluid trapped within the micropores, while the FFI was obtained as the difference between the fully saturated cumulative NMR porosity and the BVI. The microscopic storativity index (MSI) describes the ability of a micropore system to store fluid. The MSI estimated the proportion of fluid stored within the micropores of sandstone rock relative to the overall pore volume.

The mercury-injection capillary pressure (MICP) technique was conducted to determine the pore-throat distribution of sandstone samples. A Micromeritics Auto-pore IV 9400 apparatus was applied to three dry cylindrical samples of radii and length of 1.27 cm using progressive injection pressures up to 60,000 psi (450 MPa) in order to confirm the mercury invasion of the micropores. The micropore-throat modality ratio (MTMR) is a dimensionless number that relates the abundance size of the micropore throat to the macropore throat. The MTMR was used to characterize the microscopic fluid confinement (Figure 2i).

Table 2. Main parameters of NMR acquisition.

Parameter	Value
Larmor frequency	2 MHz
Echo spacing time, TE	110 μ s
Signal-to-noise ratio	150
Total number of scans	32
Number of echoes	27,272
Maximum T_2	300 ms

The sandstone samples were assessed for their microscopic confinement index (MCI) in order to determine the effectiveness of the micropore system at retaining stored fluid. The MCI is a dimensionless number that combines two parameters, namely MTMR and MSI. The sandstone samples exhibiting the highest MCI values were considered the best microscopic containment candidates for CO₂-EOR and storage processes in tight rocks. (Figure 2j).

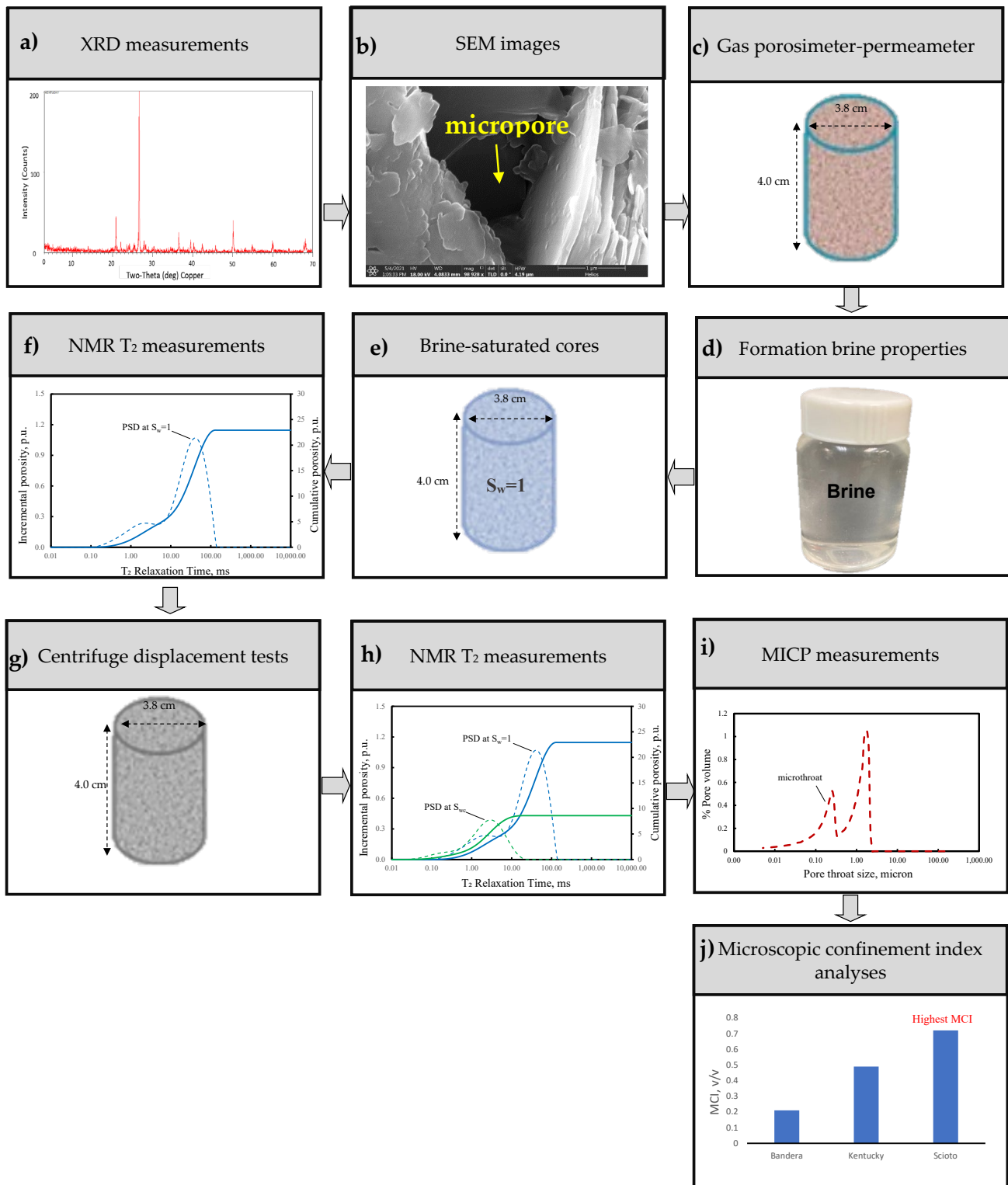


Figure 2. Workflow diagram used in this study: (a) Determine mineral contents. (b) Identify mineral grains and pore morphology. (c) Measure He porosity and N₂ permeability of sandstones. (d) Measure the density and viscosity of brine. (e) Ensure complete brine saturation of sandstones ($S_w = 1$). (f) Determine pore size distribution of brine-saturated sandstones. (g) Use air to displace brine to reach irreducible water saturation. (h) Estimate movable, bound fluid volumes and microstorativity index (MSI). (i) Estimate pore-throat distribution and micropore throat modality ratio (MTMR). (j) Identify the suitable sandstone for microscopic CO₂ injection and storage.

3. Results

An integrated approach was implemented in order to investigate the impact of the micropore system and its clay content on the pore-fluid distribution in tight sandstones. The purpose of undertaking this procedure was to determine sandstone containment and confinement. This section presents a detailed description of the experimental results and their interpretation.

3.1. Mineralogy and Morphology

We performed mineralogy and pore morphology analyses of the three sandstones using XRD and SEM techniques, respectively. XRD analysis showed that the Scioto sample had the highest quartz percentage of 89.2%, followed by 77.1% and 64.2% for Kentucky and Bandera sandstones, respectively. The findings indicated that the Bandera sandstone sample had the highest clay content at 14.3%. This was followed by the Scioto and Kentucky samples with clay contents of 4.1% and 3.6%, respectively. Table 3 summarizes the mineral composition of the tested sandstone samples.

Table 3. Mineralogical Composition of Bandera, Kentucky, and Scioto sandstone samples (units in wt%).

Sample	Quartz	Plagioclase	Orthoclase	Anhydrite	Ilmenite	Siderite	Dolomite	Halite	Hematite	Pyrite	Chlorite	Illite	Kaolinite
Bandera	64.4	12	1	3	1	0.5	0.4	1.4	1.2	0.8	3.4	6.4	4.5
Kentucky	77.1	10.2	2.8	3.6	0	0.7	0.9	0.8	0.3	0	0	3.6	0
Scioto	89.2	2.1	0.7	3	0	0.2	0	0.2	0.5	0	0.9	2.2	1

The SEM observations indicated that Bandera sandstone had sharp surfaces on account of quartz overgrowths and visible pores between elongated grains. Booklets of kaolinite and filamentous illite were observed as overlying the quartz overgrowth (Figure 3a), a phenomenon that occurred in addition to the filling of the pores with pore-filling chlorite (Figure 3b). SEM images of Scioto sandstone show visible micropores with pore-lining illite platelets coating quartz grains (Figure 3c). Images of Kentucky sandstone show booklets of kaolinite distributed abundantly in the sample (Figure 3d).

3.2. Porosity and Permeability

A routine core analysis indicated that Bandera sandstone had the highest permeability and porosity values; this was followed by Scioto sandstone and Kentucky sandstone, which were characterized by the lowest porosity and permeability values.

3.3. Pore-Fluid Distribution and Pore Structures

The microscopic confinement index (MCI) was considered in order to evaluate sandstone's microscopic storage and containment for CO₂ injection. The MCI combines MTMR and MSI parameters.

The MICP was used to assess the distribution of pore throats in the tested samples. Subsequently, we estimated the contribution of the micropore-throat system in these sandstone samples using the throat system criteria [79]. The results demonstrate that the Bandera sandstone samples exhibited a bi-modal pore-throat distribution covering micro- and macro-throat systems, with a dominant peak throat radius of approximately 6 microns. The micropore-throat system showed poor contribution to these sandstone samples compared with other sandstones, comprising around 36% of the total pore system. Kentucky and Scioto sandstones showed a bi-modal pore-throat distribution ranging from 0.02 to 2.48 microns, with a dominant peak of around 1.8 microns for both samples (Figure 4).

Although the pore-throat distribution of both Kentucky and Scioto sandstones was generally comparable, Scioto sandstone had the largest micropore-throat contribution of nearly 60% of the total pore system compared with 23.5% for Kentucky sandstone (Table 4).

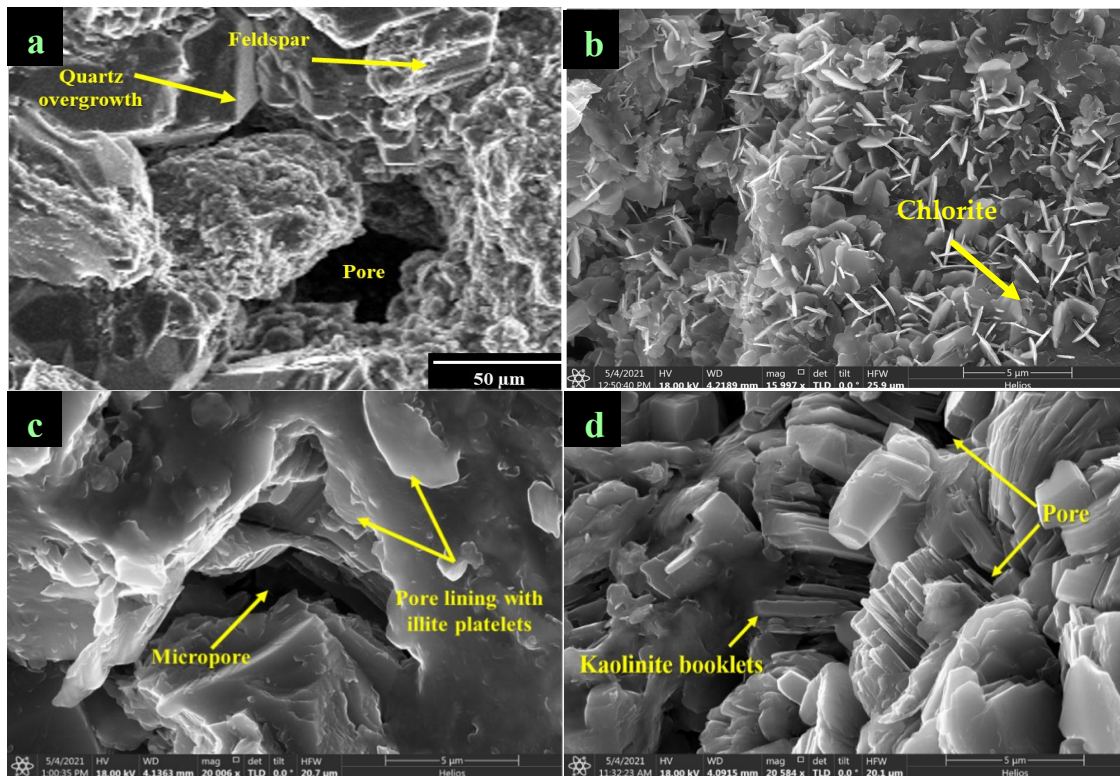


Figure 3. SEM images: (a) Bandera sandstone shows clear pores between quartz grains a top sharp surface as a result of the quartz overgrowths, and a partly weathered feldspar associated with clays. (b) Circular chlorite minerals filling the micropores are also observed in Bandera sandstone. (c) Scioto sandstone shows visible micropores associated with illite platelets. (d) Kentucky sandstone reveals books of kaolinite filling the micropores.

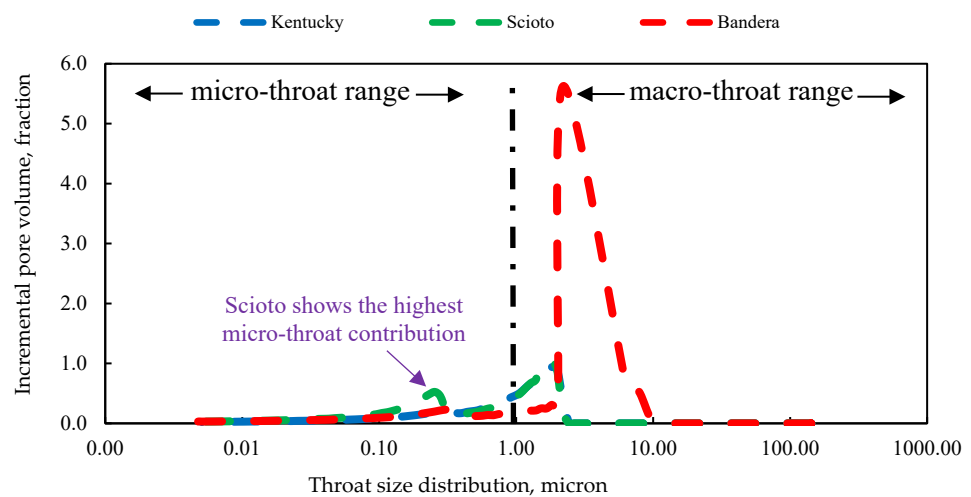


Figure 4. Pore throat distributions of the tested sandstone samples.

NMR T_2 measurements were conducted on fully brine-saturated sandstone samples in order to obtain the pore-size distribution of these sandstones (Figure 5a–c). Macropores can be identified by their high T_2 values, whereas micropores exhibit low T_2 values [80]. Results show that the Bandera sandstone had a bi-modal distribution, with T_2 values ranging from 0.1 ms to almost 140 ms. The dominant T_2 peak value representing the macropores was 40 ms, while the second peak representing the micropores was 2.5 ms (Figure 5a). Scioto and Kentucky sandstones exhibited unimodal T_2 spectra curves spanning from around

0.1 ms to approximately 100 ms, with single peak values of 35.5 ms and 25 ms, respectively (Figure 5b,c). This indicated that Scioto and Kentucky sandstones had smaller pore-size distributions than the Bandera variety, which displayed a broader T_2 distribution than that seen in Bandera sandstone (0.1–140 ms). The cumulative NMR porosities of Bandera, Scioto, and Kentucky sandstones were estimated at 22.9, 17.9, and 15.68 p.u., respectively.

Table 4. Porosity and permeability values of the tested sandstone samples. All core samples have a diameter of 3.8 ± 0.1 cm and a length of 4.0 ± 0.1 cm.

Sample	Porosity (vol.%)	Permeability (mD)
Bandera	24.4 ± 0.20	24.12 ± 1.50
Kentucky	15.0 ± 0.11	0.98 ± 0.10
Scioto	17.5 ± 0.13	1.21 ± 0.10

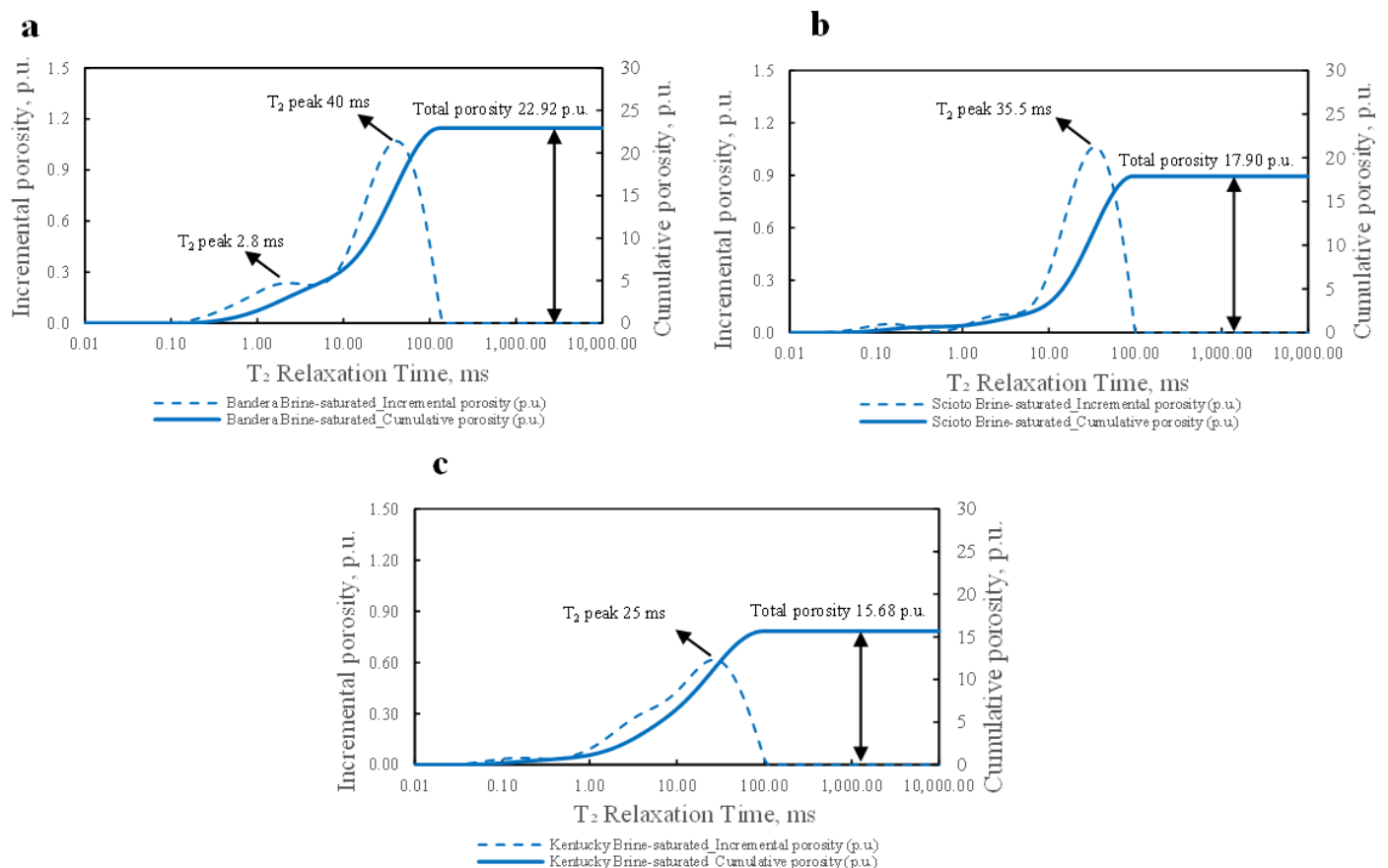


Figure 5. NMR T_2 distributions for the tested sandstone samples at brine saturation: (a) Bandera; (b) Scioto; (c) Kentucky.

NMR T_2 measurements were also conducted on partially saturated samples after centrifugation in order to determine the movable and bound-fluid contributions of the tested sandstone samples. As mentioned earlier, the movable fluid relates to macropores that are displaced easily. In contrast, the bound fluid corresponds to micropores that cannot be drained because of the capillarity and wettability forces. Figure 6a–c show the NMR T_2 measurements for brine-saturated and partially saturated conditions for the tested sandstone samples. After displacement tests, the NMR T_2 distributions of the partially saturated samples showed a unimodal distribution, varying from 0.1 ms to approximately 25 ms for Kentucky, 0.1 ms to nearly 23 ms for Bandera, and 0.1 ms to 35 ms for Scioto sandstone. These NMR spectra represented the fluid trapped in the micropore system [81].

NMR T_2 peak values exhibited shorter T_2 relaxations of 14.1 ms for Scioto, 3.2 ms for Bandera, and 3.5 ms for Kentucky. The drop in T_2 peak values indicated that pore-size distributions were reduced significantly due to the production of movable fluid from macropores. Scioto sandstone had a higher T_2 peak value (Figure 6b), indicating a large contribution from micropores compared with Kentucky and Bandera sandstones, which showed low T_2 peak values (Figure 6a,c).

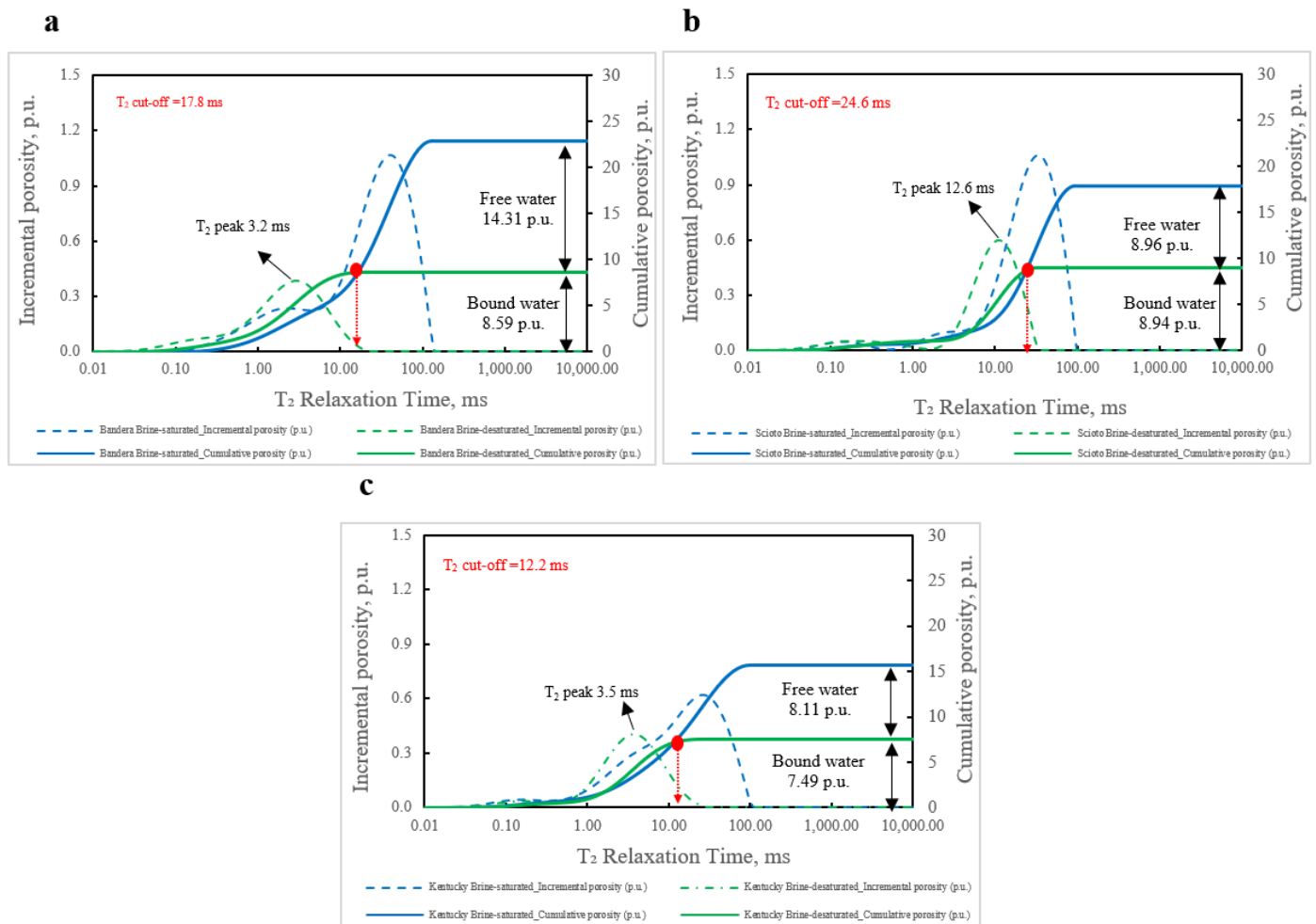


Figure 6. NMR T_2 curves of brine-saturated and post centrifuge conditions for sandstone samples of: (a) Bandera; (b) Scioto; and (c) Kentucky. Here, cumulative porosity under brine saturation (dark blue solid line); incremental porosity at full brine saturation (dark blue dashed line); cumulative porosity at partial saturation green solid line); incremental porosity at partial saturation (green dashed line); and T_2 cut-off values of each sandstone (red circles).

The T_2 cut-off value is a crucial parameter in the identification of rock bounds and movable water [82,83]. The movable water typically had a relaxation time value higher than the rock's cut-off value, while bound water exhibits a relaxation time lower than the cut-off value [84]. The T_2 cut-off value was related to rock mineralogy [85], where the threshold time for sandstone rocks ranged from 9.72 to 35.16 ms [86]. Our results demonstrate that T_2 cut-off values of the tested sandstones were 17.8, 12.2, and 24.6 ms for Bandera, Kentucky, and Scioto sandstones, respectively, which lie in the typical range for sandstone rocks (Table 4). Based on these results, we may assert that the T_2 threshold value is not always 33 ms for sandstone rocks, as recommended by other scholars [86–88]. The cumulative NMR-porosities of partial saturation conditions represent the bound-fluid volume of these sandstones. Their measurements indicated values of 8.6 p.u., 8.96 p.u., and 7.49 p.u. for Bandera, Scioto, and Kentucky sandstones, respectively (Figure 6).

3.4. Microscopic Confinement Index (MCI)

The MCI is a dimensionless value that combines the estimated storage capacity of the micropore system, as represented by the MSI parameter, and the micropore system's containment, as evaluated by the MTMR number [89]. Our calculations indicated that Scioto sandstone possessed the highest micropore system confinement with 1.44 MTMR, followed by Kentucky with 1.03 MTMR, and Bandera sandstone, which was characterized by the weakest microporosity confinement of 0.56 MTMR. CO₂ microscopic confinement index (MCI) values were calculated for the three sandstone samples tested. The results confirmed that Scioto sandstone had the highest value of 0.72 MCI, followed by Kentucky and Bandera sandstones with MCI values of 0.49 and 0.21, respectively (Table 5). The MCI was then utilized to estimate the micro-storativity index (MSI), defined as the ratio of NMR porosity at a partial saturation state to the NMR porosity at a fully brine-saturated state. MSI calculations for the three sandstone samples demonstrated that Scioto sandstone had the highest value of 0.5 MSI, followed by Kentucky sandstone with 0.48 MSI, and Bandera sandstone, which exhibited the lowest value of 0.38 MSI (Table 4).

Table 5. Summary of the micro-containment indices of three sandstones.

Sample	T ₂ Cut-Off	MSI	Micro-Throat Proportion	MTMR	MCI
	(ms)	(v/v)	(%)	(v/v)	(v/v)
Bandera	17.8	0.38	36	0.56	0.21
Kentucky	12.2	0.48	50.9	1.03	0.49
Scioto	24.6	0.50	60	1.44	0.72

Although the MSI of the Kentucky and Scioto samples showed comparable values, the difference in their calculated MCI values revealed an almost 40% difference between these two sandstones in favor of the Scioto sandstone variety. As a result, Scioto sandstone was considered to be the best candidate on account of the fact that its microscopic CO₂ confinement index was the highest among the tested sandstones.

4. Discussion

The results of the routine core analysis revealed that Bandera sandstone exhibited the best reservoir quality compared with the other samples. Conversely, Kentucky and Scioto sandstones displayed fair porosities and reasonably low permeability values (15% porosity and 0.98 mD permeability for Kentucky and 17.5% porosity and 1.21 mD permeability for Scioto) (Figure 7a). We hypothesized that the diagenetic process was accountable for the substantial decrease in the Kentucky and Scioto sandstone's permeability values. Permeability and micro-throat size proportion were found to be inversely related ($R^2 = 0.9827$, Figure 7b). This confirmed that the low permeability values of these sandstones could be ascribed to the small throat size and thereby validated the hypothesis of the diagenesis effect. Schmitt et al. [1] and Wang et al. [90] showed that high porosity values associated with low permeabilities, and vice versa, in tight sandstones arose due to the depositional conditions that led to reductions in the pore structure of the sandstone rock. Considering the complexity of the pore system in tight rocks, we advise against the use of permeability as a cut-off parameter with which to identify tight reservoirs; rather, we recommend including pore-size distribution as an essential characterization parameter in tight reservoir classifications.

It ought to be mentioned that the micropore system represented a significant proportion of the tight rock's total porosity [88,89]. Our study confirmed that the micropore systems of the studied sandstones significantly contributed to overall sandstone porosity, with contributions of 38% in the Bandera, 48% in the Kentucky, and 50% in the Scioto samples. These results are consistent with those of Lai et al. [85], who reported that bound-fluid contribution (micropore system) can account for up to 60% of the total pore system. Thus, it is more convenient to investigate the relationship between the micropore system and

the pore-fluid distribution in tight sandstones in order to enable geologists and petroleum engineers to improve the efficiency of CO₂ injection into the micropores of tight rocks. Bandera sandstone possesses a wider pore-size distribution than other sandstones, with values ranging from 0.1 ms to 140 ms, as yielded by our NMR analyses (Figure 5a). Furthermore, the NMR findings show that 62% of Bandera sandstone's pore-fluid distribution is mobile (within the macropore system). This finding aligns with the MICP outcomes, demonstrating that Bandera sandstone's significant contribution to flow comes from the macropore throat system (64%) ($R^2 = 0.9006$, Figure 8). Additionally, SEM images illustrate that Bandera sandstone contains visible macropores (Figure 3a). The SEM findings also show the presence of clay-coated grains, which inhibit quartz overgrowth and hence preserve the macropore system [91,92]. Consequently, the combination of the above findings leads us to conclude that Bandera sandstone demonstrates, by comparison, the highest proportion of a macropore system (Figure 8). The low contribution of the micropore system in Bandera sandstone is attributed to the presence of clay minerals, including kaolinite booklets, chlorite, and fibrous illite minerals, which tend to clog throats and fill pores and therefore cause a significant reduction in the micropore system (the lowest micropore system among the tested samples was 38% to the total pore system) (Table 4). Furthermore, negative correlations can be observed between the clay mineral content and the bound-fluid contribution represented by the micropore system, as derived from the NMR analyses ($R^2 = 0.9726$, Figure 9a) and micropore-throat proportion ($R^2 = 0.781$, Figure 9b). Hence, the low clay content of the other sandstones (50.1% for Scioto and 48% for Kentucky) leads to the presence of high micropore-system proportions, and to the relatively high contribution of the micropore-throat system (60% for Scioto and 50.9% for Kentucky sandstone).

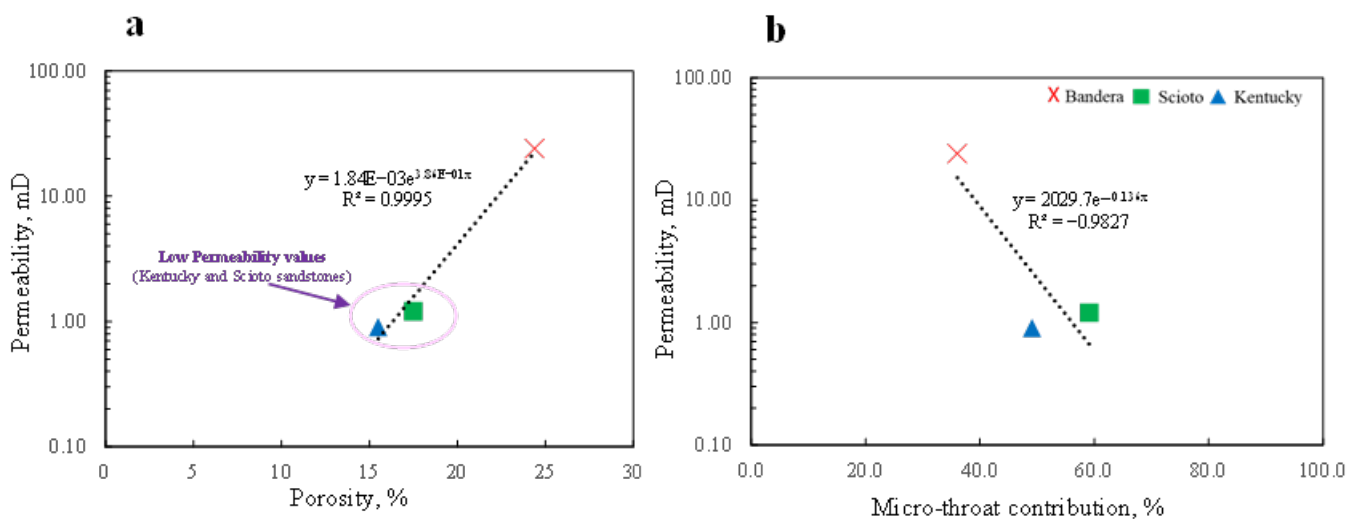


Figure 7. Cross-plots demonstrating the relation between permeability to porosity and micro-pore throat contribution in tested sandstones; (a) the cross-plots between permeability and porosity; (b) the cross-plots between permeability and micro-throat contribution.

In our research, a strong inverse relationship was found between the illite clay mineral and the micro-throat proportion for the tested sandstones, indicating that the contribution of the micropore-throat system decreases as illite clay content increases ($R^2 = 0.9875$, s 9f). We also demonstrated that chlorite and kaolinite clay minerals have less of an effect on the micropore-throat proportion compared with illite minerals ($R^2 = 0.625$ for chlorite and $R^2 = 0.581$ for kaolinite) (Figure 9h,d). Based on the above findings, we believe that injected fluids can access the tiny pores as long as the rock's micropore system suits the newly established index, known as the microscopic containment index (MCI). The MCI can be used to evaluate the micropore system of the tested sandstones, taking into account both the micropore system confinement and storativity. The confinement of the micropore system is calculated based on the MTMR [93], whereas the micropore system's storativity

is estimated as the ratio of the NMR porosity at a partial saturation condition to the NMR porosity at a fully brine-saturated state. A high MCI value implies that the micropore system in tight rocks is suitable for use in microscopic CO₂ injection on account of its high storage capacity and well-confined micropore system. On the contrary, low MCI values demonstrate that the sandstone micropore system exhibits limited capacity; additionally, inadequate fluid containment makes this system unsuitable for microscopic CO₂ injection. The MCI analyses were compared to the results of the containment and storativity of the tested sandstone samples, and the results showed a direct relationship ($R^2 = 0.8478$ for micro-storativity (Figure 10a) and $R^2 = 0.9976$ for micro-containment (Figure 10b)). This relationship confirmed that the MCI increases as the storativity and containment of the micropore system increase. For the tight sandstones analyzed, the results show that the MCI of Scioto sandstone was the highest among the tested sandstone samples with a value of 0.72, and this is attributed to the great capacity of the Scioto sandstone's micropore system of 0.5 MSI and the excellent micropore system confinement of 1.44 MTMR, suggesting that Scioto sandstone is a suitable candidate for microscopic CO₂ injection. The low contribution of micro-storativity and containment in Bandera sandstone of 0.38 MSI and 0.56 MTMR, respectively, led to a significant reduction in the microscopic containment index to 0.38 MCI; therefore, Bandera is not recommended for use in macroscopic CO₂ injection.

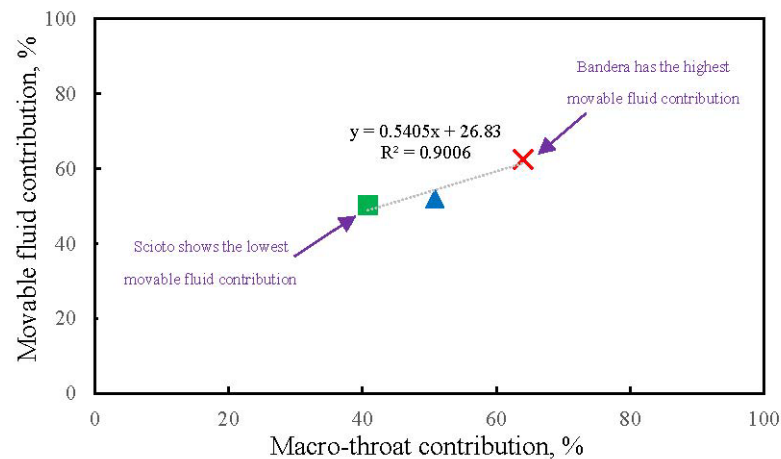


Figure 8. Cross-plot showing the relation between movable fluid contribution and macro-throat proportion for the three tested sandstones.

If a researcher wishes to gain a deeper insight into this relationship between the MCI results and micro-storativity and micro-confinement indices, it is more convenient to focus on the factors impacting these indices. The increase in the micropore-throat proportions results in an increase in the storage capacity of the micropore system in the examined sandstones ($R^2 = 0.9006$, Figure 11a), a phenomenon which can be related to the significant influence of clay minerals on the micropore system as a result of diagenetic alteration [89]. Furthermore, the reduction in the micropore's storativity proportion is related to the increase in the clay mineral content ($R^2 = 0.9726$, Figure 11b), and this is in line with the fact that the fibrous illite and booklets of kaolinite clay minerals can act as pore-bridging and pore-filling substances, respectively. These processes reduce the existing micropore system and thus affect the bound-fluid contribution [94].

Our analysis further shows that the percentage of micropore throat in the tested sandstones is strongly correlated to the micropore's containment ($R^2 = 0.9836$, Figure 12a). This can be explained by the fact that smaller throat diameters can lead to greater capillary pressures, preventing fluid mobilization within the pore system [95]. In our results, compared with the relation between the total clay content and the micropore system storativity index ($R^2 = 0.9726$, Figure 11b), a fair relation was found between the total clay content and micropore system containment ($R^2 = 0.666$, Figure 12b). Gathering a larger dataset would provide a more in-depth understanding of our newly discovered dimensionless numbers;

however, these outcrops from which the samples were obtained are known for their clean and very homogeneous nature. This presents a potential area for future research based on our current findings.

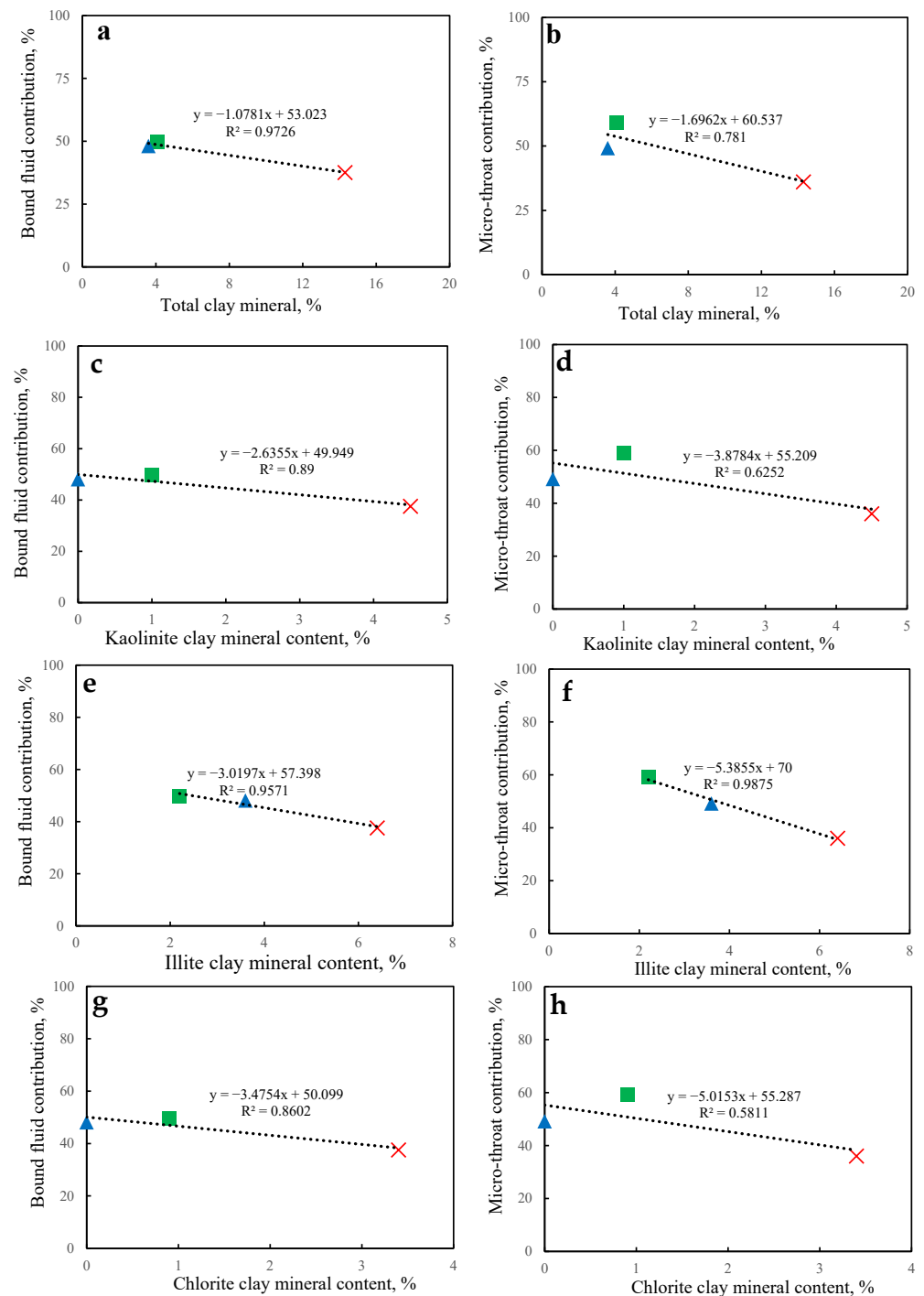


Figure 9. Cross-plots showing the relation between bound-fluid contribution, micro-throat proportion and clay mineral content in tested sandstones: (a) cross-plots between bound-fluid contribution and total clay mineral content; (b) cross-plots between micro-throat contribution and clay mineral content; (c) cross-plots between bound-fluid contribution and kaolinite clay content; (d) cross-plots between micro-throat contribution and kaolinite clay content; (e) cross-plots between bound-fluid contribution and illite clay content; (f) cross-plots between micro-throat contribution and illite clay content; (g) cross-plots between bound-fluid contribution and chlorite clay content; (h) cross-plots between micropore throat-size proportion and chlorite clay content.

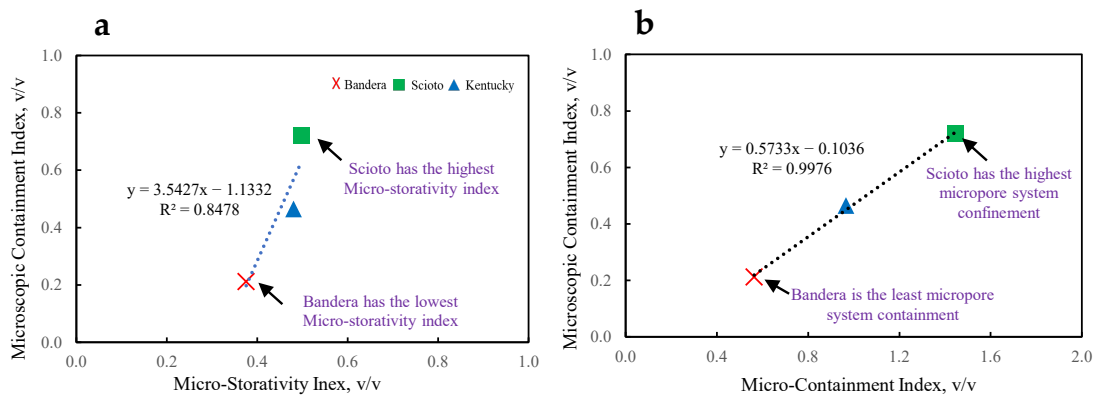


Figure 10. Cross-plots showing the relation between (a) the microscopic containment index and the micro-storativity index; and (b) the microscopic confinement index and the micro-containment index of the tested sandstones.

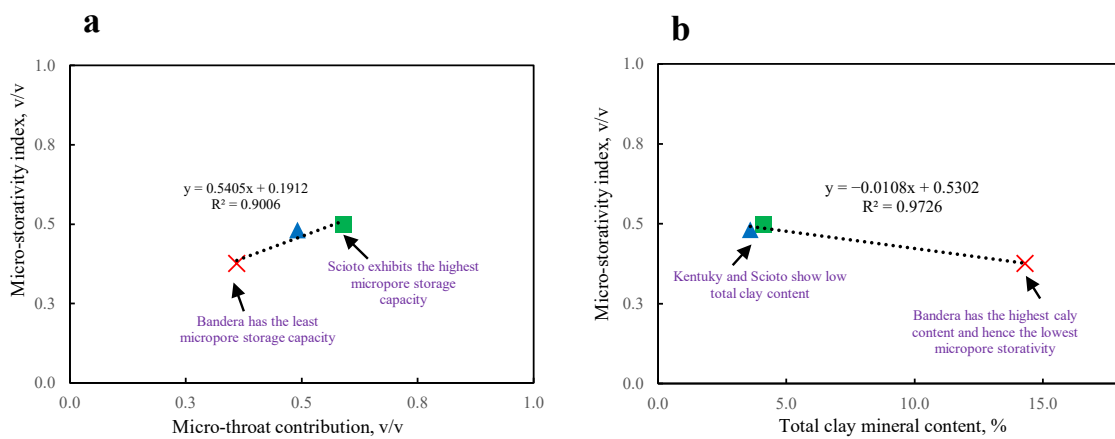


Figure 11. Cross-plots showing the relation of micro-storativity index to the micro-throat proportion, total clay mineral content in tight sandstone samples: (a) cross-plots showing the relation of micro-storativity index to micro-throat proportion; (b) cross-plots showing the relation of micro-storativity index to total mineral content (the trendlines show the relation between measurements).

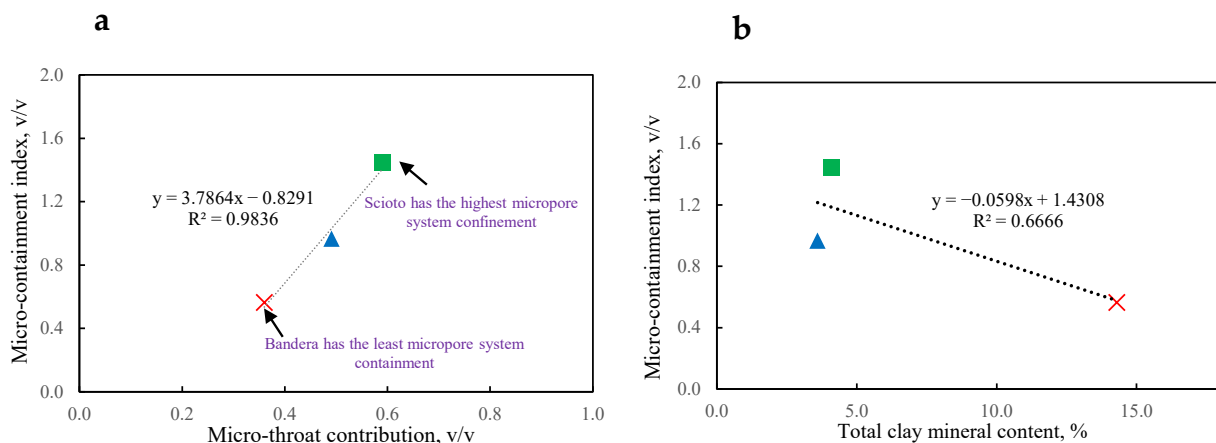


Figure 12. Cross-plots showing the relation of the micro-containment index to the micro-throat proportion and total clay mineral content in tight sandstone samples: (a) cross-plots showing the relation of the micro-containment index to the micro-throat proportion; (b) cross-plots showing the relation of the micro-containment index to the total clay mineral content (the trendlines show the relation between measurements).

5. Conclusions

This study focused on determining pore-fluid distribution and investigated its impact on the tight sandstones' micropore system. A new dimensionless number, termed the MCI, was developed to select a suitable tight sandstone for CO₂ injection and storage. Based on the findings obtained, the following conclusions were derived:

- The findings indicated that the Bandera sandstone sample had the highest clay content, followed by the Scioto and Kentucky sandstone samples. Nevertheless, a routine core analysis indicated that Bandera sandstone had the highest permeability and porosity values followed by Scioto sandstone and, finally, by Kentucky sandstone, which had with the lowest porosity and permeability values.
- SEM analyses indicated Bandera sandstone to be characterized by quartz overgrowths and booklets of kaolinite and filamentous illite overlying the quartz in addition to pore-filling chlorite filling the pores. Scioto sandstone showed visible micropores with pore-lining illite platelets coating the quartz grains, while Kentucky sandstone showed an abundant distribution of booklets of kaolinite.
- The MICP results demonstrated that all sandstone samples exhibited a bi-modal pore-throat distribution covering micro- and macropore throat systems. The Bandera sandstone micropore-throat system showed poor contribution, while Scioto sandstone made the largest micropore-throat contribution to the total pore system.
- NMR T₂ measurements conducted on partially saturated samples after the displacement tests reveal longer T₂ relaxations for Scioto and comparable values for Bandera and Kentucky sandstones, indicating a large contribution from Scioto micropores compared with Kentucky and Bandera sandstones.
- Bandera sandstone's micropore system's ability to store and confine fluid or gas was found to be the weakest among the tested sandstone samples. The low contribution values of the storativity and confinement of the micropore system in Bandera sandstone could be attributed to the presence of clay mineral content. In particular, this could be explained by the presence of pore-filling kaolinite booklets, which significantly reduced the micropore storativity, and the presence of pore-bridging fibrous illite, which reduced the micropore-throat proportion and, hence, reduced the confinement of the micropore system.
- A strong positive correlation was obtained between the micro-throat proportion and the micro-confinement contribution in the tested sandstone samples, indicating that the higher the micro-throat contribution in the pore system was, the more confined the micropore system became.
- The MCI indicated that Scioto sandstone was a suitable candidate for microscopic CO₂ injection and storage due to its high contributions of micropore confinement and storativity compared with the other tested samples; these factors will improve CO₂ injectivity in the micropore system of tight sandstones.

Author Contributions: H.A.: Writing, Organization, Experiments. K.-H.W.: Supervision, Methodology, Investigation and Writing—review and editing. M.M.: Methodology and Data discussion. A.A.: Data investigation and Writing—review and editing. M.A.: Methodology and Data investigation. P.Z.: Supervision, Project administration, Data discussion, Methodology, and Writing—review and editing. All authors have read and agreed to the published version of the manuscript.

Funding: This research received no external funding.

Acknowledgments: The authors would like to thank Ivan Deshnenkov and Naif Alqahtani for their support and insightful conversations regarding this study. Furthermore, we acknowledge the participation of Hyung Kwak, Mustafa Satrawi, and Jun Gao for their help and support in the NMR measurements. Additionally, the authors thank Essa Abdullah, Abdulkareem AlRadwan, and Hussain Al Ali for their insightful conversations on the petrophysical analyses.

Conflicts of Interest: The authors declare no conflict of interest.

References

1. Schmitt, M.; Fernandes, C.P.; Wolf, F.G.; Neto, J.A.B.D.C.; Rahner, C.P.; dos Santos, V.S.S. Characterization of Brazilian tight gas sandstones relating permeability and Angstrom-to-micron-scale pore structures. *J. Nat. Gas Sci. Eng.* **2015**, *27*, 785–807. [CrossRef]
2. Zheng, D.; Pang, X.; Jiang, F.; Liu, T.; Shao, X.; Huyan, Y. Characteristics and controlling factors of tight sandstone gas reservoirs in the Upper Paleozoic strata of Linxing area in the Ordos Basin, China. *J. Nat. Gas Sci. Eng.* **2020**, *75*, 103135. [CrossRef]
3. U.S. Energy Information Administration (EIA). *Monthly Energy Review June 2022*; U.S. Energy Information Administration (EIA): Washington, DC, USA, 2022.
4. McGlade, C.; Speirs, J.; Sorrell, S. Unconventional gas—A review of regional and global resource estimates. *Energy* **2013**, *55*, 571–584. [CrossRef]
5. Wang, J.; Feng, L.; Steve, M.; Tang, X.; Gail, T.E.; Mikael, H. China's unconventional oil: A review of its resources and outlook for long-term production. *Energy* **2015**, *82*, 31–42. [CrossRef]
6. Gao, H.; Li, H. Determination of movable fluid percentage and movable fluid porosity in ultra-low permeability sandstone using nuclear magnetic resonance (NMR) technique. *J. Pet. Sci. Eng.* **2015**, *133*, 258–267. [CrossRef]
7. Alam, S. Potential of Tight Gas in Pakistan: Productive, Economic and Policy Aspects. In Proceedings of the Annual Technical Conference of Pakistan Association of Petroleum Geoscientists (PAPG), Islamabad, Pakistan, 10–11 November 2010.
8. Naik, G.C. Tight Gas Reservoir an Unconventional Natural Energy Source for the Future. 2004. Available online: http://www.pinedaleonline.com/socioeconomic/pdfs/tight_gas.pdf (accessed on 10 February 2022).
9. U.S. Government Accountability Office (GAO). *Impacts of Potential Oil Shale Development on Water Resources*; U.S. Government Accountability Office (GAO): Washington, DC, USA, 2011.
10. National Resources Canada. North American Tight Oil. 2012. Available online: <http://www.nrcan.gc.ca/energy/sources/crude/2114#oil1> (accessed on 10 February 2022).
11. Holditch, S.A. Tight gas sands. *J. Pet. Technol.* **2006**, *58*, 86–93. [CrossRef]
12. Worden, R.H.; Burley, S.D. Sandstone diagenesis: The evolution of sand to stone. In *Sandstone Diagenesis: Recent and Ancient*; International Association of Sedimentologists Special Publication 4; Blackwell: Oxford, UK, 2003; pp. 1–44.
13. Xiao, D.; Lu, Z.; Jiang, S.; Lu, S. Comparison and integration of experimental methods to characterize the full-range pore features of tight gas sandstone—A case study in Songliao Basin of China. *J. Nat. Gas Sci. Eng.* **2016**, *34*, 1412–1421. [CrossRef]
14. Yue, D.; Wu, S.; Xu, Z.; Xiong, L.; Chen, D.; Ji, Y.; Zhou, Y. Reservoir quality, natural fractures, and gas productivity of upper Triassic Xujiahe tight gas sandstones in western Sichuan Basin, China. *Mar. Pet. Geol.* **2018**, *89*, 370–386. [CrossRef]
15. Zhang, L.; Lu, S.; Xiao, D.; Li, B. Pore structure characteristics of tight sandstones in the northern Songliao Basin, China. *Mar. Pet. Geol.* **2017**, *88*, 170–180. [CrossRef]
16. Cao, Y.; Tang, M.; Zhang, Q.; Tang, J.; Lu, S. Dynamic capillary pressure analysis of tight sandstone based on digital rock model. *Capillarity* **2020**, *3*, 28–35. [CrossRef]
17. Nabawy, B.S.; Khalil, H.M.; Fathy, M.S.; Ali, F. Impacts of microfacies type on reservoir quality and pore fabric anisotropy of the Nubia sandstone in the central Eastern Desert, Egypt. *Geol. J.* **2020**, *55*, 4507–4524. [CrossRef]
18. Syed, F.I.; Dahaghi, A.K.; Muther, T. Laboratory to field scale assessment for EOR applicability in tight oil reservoirs. *Pet. Sci.* **2022**, *19*, 2131–2149. [CrossRef]
19. Edwards, A.C. Grain size and sorting in modern beach sands. *J. Coast. Res.* **2001**, *17*, 38–52.
20. Li, L.; Su, Y.; Sheng, J.J.; Hao, Y.; Wang, W.; Lv, Y.; Zhao, Q.; Wang, H. Experimental and numerical study on CO₂ sweep volume during CO₂ huff-n-puff enhanced oil recovery process in shale oil reservoirs. *Energy Fuels* **2019**, *33*, 4017–4032. [CrossRef]
21. Bjørlykke, K. Relationships between depositional environments, burial history and rock properties. Some principal aspects of diagenetic process in sedimentary basins. *Sediment. Geol.* **2014**, *301*, 1–14. [CrossRef]
22. Bjørlykke, K.; Jahren, J. Open or closed geochemical systems during diagenesis in sedimentary basins: Constraints on mass transfer during diagenesis and the prediction of porosity in sandstone and carbonate reservoirs. *AAPG Bull.* **2012**, *96*, 2193–2214. [CrossRef]
23. Bultreys, T.; De Boever, W.; Cnudde, V. Imaging and image-based fluid transport modeling at the pore scale in geological materials: A practical introduction to the current state-of-the-art. *Earth-Science Rev.* **2016**, *155*, 93–128. [CrossRef]
24. Endres, A.L.; Knight, R. The effects of pore-scale fluid distribution on the physical properties of partially saturated tight sandstones. *J. Appl. Phys.* **1991**, *69*, 1091–1098. [CrossRef]
25. Song, X.; Guo, Y.; Zhang, J.; Sun, N.; Shen, G.; Chang, X.; Yu, W.; Tang, Z.; Chen, W.; Wei, W.; et al. Fracturing with carbon dioxide: From microscopic mechanism to reservoir application. *Joule* **2019**, *3*, 1913–1926. [CrossRef]
26. Holm, L.W.; Josendal, V.A. Mechanisms of oil displacement by carbon dioxide. *J. Pet. Technol.* **1974**, *26*, 1427–1438. [CrossRef]
27. Yang, Y.; Zhou, Y.; Blunt, M.J.; Yao, J.; Cai, J. Advances in multiscale numerical and experimental approaches for multiphysics problems in porous media. *Adv. Geo-Energy Res.* **2021**, *5*, 233–238. [CrossRef]
28. Juanes, R.; Spiteri, E.J.; Orr, F.M., Jr.; Blunt, M.J. Impact of relative permeability hysteresis on geological CO₂ storage. *Water Resour. Res.* **2006**, *42*, W12418. [CrossRef]
29. Zhang, X.; Wei, B.; Shang, J.; Gao, K.; Pu, W.; Xu, X.; Wood, C.; Sun, L. Alterations of geochemical properties of a tight sandstone reservoir caused by supercritical CO₂-brine-rock interactions in CO₂-EOR and geosequestration. *J. CO₂ Util.* **2018**, *28*, 408–418. [CrossRef]

30. Payton, R.L.; Fellgett, M.; Clark, B.L.; Chiarella, D.; Kingdon, A.; Hier-Majumder, S. Pore-scale assessment of subsurface carbon storage potential: Implications for the UK Geoenery Observatories project. *Pet. Geosci.* **2021**, *27*, petgeo2020-092. [[CrossRef](#)]
31. Bjørlykke, K.; Høeg, K. Effects of burial diagenesis on stresses, compaction and fluid flow in sedimentary basins. *Mar. Pet. Geol.* **1997**, *14*, 267–276. [[CrossRef](#)]
32. Selley, R.C. *Applied Sedimentology*; Elsevier: Amsterdam, The Netherlands, 2000.
33. Loucks, R.G.; Reed, R.M.; Ruppel, S.C.; Jarvie, D.M. Morphology, genesis, and distribution of nanometer-scale pores in siliceous mudstones of the Mississippian Barnett Shale. *J. Sediment. Res.* **2009**, *79*, 848–861. [[CrossRef](#)]
34. Pittman, E.D. *Porosity, Diagenesis, and Productive Capability of Sandstone Reservoirs*; The Society of Economic Paleontologists and Mineralogists (SEPM): Tulsa, OK, USA, 1979.
35. Worden, R.H.; Griffiths, J.; Wooldridge, L.J.; Utley, J.E.P.; Lawan, A.Y.; Muhammed, D.D.; Simon, N.; Armitage, P. Chlorite in sandstones. *Earth-Sci. Rev.* **2020**, *204*, 103105. [[CrossRef](#)]
36. Chang, J.; Fan, X.; Jiang, Z.; Wang, X.; Chen, L.; Li, J.; Zhu, L.; Wan, C.; Chen, Z. Differential impact of clay minerals and organic matter on pore structure and its fractal characteristics of marine and continental shales in China. *Appl. Clay Sci.* **2022**, *216*, 106334. [[CrossRef](#)]
37. McLean, R.F.; Kirk, R.M. Relationships between grain size, size-sorting, and foreshore slope on mixed sand-shingle beaches. *N. Z. J. Geol. Geophys.* **1969**, *12*, 138–155. [[CrossRef](#)]
38. Keelan, D.K. Core analysis for aid in reservoir description. *J. Pet. Technol.* **1982**, *34*, 2483–2491. [[CrossRef](#)]
39. Islam, M.A. Diagenesis and reservoir quality of Bhuban sandstones (Neogene), Titas gas field, Bengal Basin, Bangladesh. *J. Asian Earth Sci.* **2009**, *35*, 89–100. [[CrossRef](#)]
40. Hollis, C.; Vahrenkamp, V.; Tull, S.; Mookerjee, A.; Taberner, C.; Huang, Y. Pore system characterisation in heterogeneous carbonates: An alternative approach to widely-used rock-typing methodologies. *Mar. Pet. Geol.* **2010**, *27*, 772–793. [[CrossRef](#)]
41. Beard, D.C.; Weyl, P.K. Influence of texture on porosity and permeability of unconsolidated sand. *AAPG Bull.* **1973**, *57*, 349–369.
42. Chima, P.; Baiyegunhi, C.; Liu, K.; Gwavava, O. Diagenesis and rock properties of sandstones from the Stormberg Group, Karoo Supergroup in the Eastern Cape Province of South Africa. *Open Geosci.* **2018**, *10*, 740–771. [[CrossRef](#)]
43. Ajdukiewicz, J.M.; Lander, R.H. Sandstone reservoir quality prediction: The state of the art. *AAPG Bull.* **2010**, *94*, 1083–1091. [[CrossRef](#)]
44. Makeen, Y.M.; Abdullah, W.H.; Ayinla, H.A.; Hakimi, M.H.; Sia, S.-G. Sedimentology, diagenesis and reservoir quality of the upper Abu Gabra Formation sandstones in the Fula Sub-basin, Muglad Basin, Sudan. *Mar. Pet. Geol.* **2016**, *77*, 1227–1242. [[CrossRef](#)]
45. McKinley, J.M.; Atkinson, P.M.; Lloyd, C.D.; Ruffell, A.H.; Worden, R.H. How porosity and permeability vary spatially with grain size, sorting, cement volume, and mineral dissolution in fluvial Triassic sandstones: The value of geostatistics and local regression. *J. Sediment. Res.* **2011**, *81*, 844–858. [[CrossRef](#)]
46. Mozley, P.S.; Heath, J.E.; Dewers, T.A.; Bauer, S.J. Origin and heterogeneity of pore sizes in the Mount Simon Sandstone and Eau Claire Formation: Implications for multiphase fluid flow. *Geosphere* **2016**, *12*, 1341–1361. [[CrossRef](#)]
47. Kashif, M.; Cao, Y.; Yuan, G.; Asif, M.; Javed, K.; Mendez, J.N.; Khan, D.; Miruo, L. Pore size distribution, their geometry and connectivity in deeply buried Paleogene Es1 sandstone reservoir, Nanpu Sag, East China. *Pet. Sci.* **2019**, *16*, 981–1000. [[CrossRef](#)]
48. Zhiyong, G.; Jiarui, F.; Jinggang, C.; Xiaoqi, W.; Chuanmin, Z.; Yuxin, S. Physical simulation and quantitative calculation of increased feldspar dissolution pores in deep reservoirs. *Pet. Explor. Dev.* **2017**, *44*, 387–398.
49. Shao, X.; Pang, X.; Jiang, F.; Li, L.; Li, H.; Zheng, D.; Huyan, Y. Genesis and accumulation of natural gas in the Upper Palaeozoic strata of north-eastern Ordos Basin, China. *Geol. J.* **2019**, *54*, 3212–3225. [[CrossRef](#)]
50. Neasham, J.W. The morphology of dispersed clay in sandstone reservoirs and its effect on sandstone shaliness, pore space and fluid flow properties. In *SPE Annual Fall Technical Conference and Exhibition*; OnePetro: Richardson, TX, USA, 1977.
51. Schrader, M.E.; Yariv, S. Wettability of clay minerals. *J. Colloid Interface Sci.* **1990**, *136*, 85–94. [[CrossRef](#)]
52. Schoonheydt, R.A.; Johnston, C.T. Surface and interface chemistry of clay minerals. *Dev. Clay Sci.* **2006**, *1*, 87–113.
53. Yuan, G.; Gluyas, J.; Cao, Y.; Oxtoby, N.H.; Jia, Z.; Wang, Y.; Xi, K.; Li, X. Diagenesis and reservoir quality evolution of the Eocene sandstones in the northern Dongying Sag, Bohai Bay Basin, East China. *Mar. Pet. Geol.* **2015**, *62*, 77–89. [[CrossRef](#)]
54. Kuila, U.; Prasad, M. Specific surface area and pore-size distribution in clays and shales. *Geophys. Prospect.* **2013**, *61*, 341–362. [[CrossRef](#)]
55. Wilson, L.; Wilson, M.J.; Green, J.; Patey, I. The influence of clay mineralogy on formation damage in North Sea reservoir sandstones: A review with illustrative examples. *Earth-Sci. Rev.* **2014**, *134*, 70–80. [[CrossRef](#)]
56. Kassab, M.A.; Abu Hashish, M.F.; Nabawy, B.S.; Elnaggar, O.M. Effect of kaolinite as a key factor controlling the petrophysical properties of the Nubia sandstone in central Eastern Desert, Egypt. *J. Afr. Earth Sci.* **2017**, *125*, 103–117. [[CrossRef](#)]
57. Rosenbrand, E.; Fabricius, I.L.; Fisher, Q.; Grattoni, C. Permeability in Rotliegend gas sandstones to gas and brine as predicted from NMR, mercury injection and image analysis. *Mar. Pet. Geol.* **2015**, *64*, 189–202. [[CrossRef](#)]
58. Bjorkum, P.A. How important is pressure in causing dissolution of quartz in sandstones? *J. Sediment. Res.* **1996**, *66*, 147–154.
59. Anovitz, L.M.; Cole, D.R. Characterization and analysis of porosity and pore structures. *Rev. Miner. Geochem.* **2015**, *80*, 61–164. [[CrossRef](#)]
60. Al Saadi, F.; Wolf, K.-H.; Van Kruijsdijk, C. Characterization of Fontainebleau sandstone: Quartz overgrowth and its impact on pore-throat framework. *J. Pet. Environ. Biotechnol.* **2017**, *8*, 1–12. [[CrossRef](#)]

61. Bloch, S.; Lander, R.H.; Bonnell, L.M. Anomalous high porosity and permeability in deeply buried sandstone reservoirs: Origin and predictability. *AAPG Bull.* **2002**, *86*, 301–328.
62. Freiburg, J.T.; Ritz, R.W.; Kehoe, K.S. Depositional and diagenetic controls on anomalously high porosity within a deeply buried CO₂ storage reservoir—The Cambrian Mt. Simon sandstone, Illinois basin, USA. *Int. J. Greenh. Gas Control.* **2016**, *55*, 42–54. [[CrossRef](#)]
63. Wu, Y.; Tahmasebi, P.; Lin, C.; Zahid, M.A.; Dong, C.; Golab, A.N.; Ren, L. A comprehensive study on geometric, topological and fractal characterizations of pore systems in low-permeability reservoirs based on SEM, MICP, NMR, and X-ray CT experiments. *Mar. Pet. Geol.* **2019**, *103*, 12–28. [[CrossRef](#)]
64. Wu, K.; Chen, D.; Zhang, W.; Yang, H.; Wu, H.; Cheng, X.; Qu, Y.; He, M. Movable Fluid Distribution Characteristics and Microscopic Mechanism of Tight Reservoir in Yanchang Formation, Ordos Basin. *Advances in the Exploration and Development of Unconventional Oil and Gas: From the Integration of Geology and Engineering.* *Front. Earth Sci.* **2022**, *10*, 840875. [[CrossRef](#)]
65. Kleinberg, R.L.; Kenyon, W.E.; Mitra, P.P. Mechanism of NMR relaxation of fluids in rock. *J. Magn. Reson. Ser. A* **1994**, *108*, 206–214. [[CrossRef](#)]
66. Coates, G.R.; Xiao, L.Z.; Prammer, M.G. *NMR Logging Principles and Applications*; Gulf Publishing Company: Houston, TX, USA, 1999.
67. Hirasaki, G.J.; Huang, C.C.; Zhang, G.Q. Interpretation of wettability in sandstones with NMR analysis. *Petrophys.-SPWLA J. Form. Eval. Reserv. Descr.* **2000**, *41*, 223–233.
68. Dunn, K.J.; Bergman, D.J.; LaTorraca, G.A. (Eds.) *Nuclear Magnetic Resonance: Petrophysical and Logging Applications*; Elsevier: Amsterdam, The Netherlands, 2002.
69. Baban, A.; Al-Yaseri, A.; Keshavarz, A.; Amin, R.; Iglauer, S. CO₂—brine—sandstone wettability evaluation at reservoir conditions via Nuclear Magnetic Resonance measurements. *Int. J. Greenh. Gas Control.* **2021**, *111*, 103435. [[CrossRef](#)]
70. Dutton, S.P.; Loucks, R.G. Diagenetic controls on evolution of porosity and permeability in lower Tertiary Wilcox sandstones from shallow to ultradeep (200–6700 m) burial, Gulf of Mexico Basin, USA. *Mar. Pet. Geol.* **2010**, *27*, 69–81. [[CrossRef](#)]
71. Nelson, P.H. Pore-throat sizes in sandstones, tight sandstones, and shales. *AAPG Bull.* **2009**, *93*, 329–340. [[CrossRef](#)]
72. Mørk, M.B.E. Diagenesis and quartz cement distribution of low-permeability Upper Triassic–Middle Jurassic reservoir sandstones, Longyearbyen CO₂ lab well site in Svalbard, Norway. *AAPG Bull.* **2013**, *97*, 577–596. [[CrossRef](#)]
73. Dai, J.; Ni, Y.; Hu, G.; Huang, S.; Liao, F.; Yu, C.; Gong, D.; Wu, W. Stable carbon and hydrogen isotopes of gases from the large tight gas fields in China. *Sci. China Earth Sci.* **2014**, *57*, 88–103. [[CrossRef](#)]
74. Pan, B.; Yin, X.; Ju, Y.; Iglauer, S. Underground hydrogen storage: Influencing parameters and future outlook. *Adv. Colloid Interface Sci.* **2021**, *294*, 102473. [[CrossRef](#)]
75. Peksa, A.E.; Wolf, K.-H.A.; Zitha, P.L. Bentheimer sandstone revisited for experimental purposes. *Mar. Pet. Geol.* **2015**, *67*, 701–719. [[CrossRef](#)]
76. Huyan, Y.; Pang, X.; Jiang, F.; Li, L.; Zheng, D.; Shao, X. Coupling relationship between tight sandstone reservoir and gas charging: An example from lower Permian Taiyuan Formation in Kangning field, northeastern Ordos Basin, China. *Mar. Pet. Geol.* **2019**, *105*, 238–250. [[CrossRef](#)]
77. Kenyon, W.E. Petrophysical principles of applications of NMR logging. *Log Anal.* **1997**, *38*, 21–43.
78. Carr, H.Y.; Purcell, E.M. Effects of diffusion on free precession in nuclear magnetic resonance experiments. *Phys. Rev.* **1954**, *94*, 630–638. [[CrossRef](#)]
79. Xiao, L.; Liu, X.-P.; Zou, C.-C.; Hu, X.-X.; Mao, Z.-Q.; Shi, Y.-J.; Guo, H.-P.; Li, G.-R. Comparative study of models for predicting permeability from nuclear magnetic resonance (NMR) logs in two Chinese tight sandstone reservoirs. *Acta Geophys.* **2014**, *62*, 116–141. [[CrossRef](#)]
80. Song, Y.-Q. Pore sizes and pore connectivity in rocks using the effect of internal field. *Magn. Reson. Imaging* **2001**, *19*, 417–421. [[CrossRef](#)]
81. Miller, M.N.; Paltiel, Z.; Gillen, M.E.; Granot, J.; Bouton, J.C. Spin echo magnetic resonance logging: Porosity and free fluid index determination. In *SPE Annual Technical Conference and Exhibition*; OnePetro: Richardson, TX, USA, 1990.
82. Looyestijn, W.J. Wettability index determination from NMR logs. *Petrophys.-SPWLA J. Form. Eval. Reserv. Descr.* **2008**, *49*, 130–145.
83. Mitchell, J.; Fordham, E.J. Contributed Review: Nuclear magnetic resonance core analysis at 0.3 T. *Rev. Sci. Instrum.* **2014**, *85*, 111502. [[CrossRef](#)] [[PubMed](#)]
84. Elsayed, M.; Isah, A.; Hiba, M.; Hassan, A.; Al-Garadi, K.; Mahmoud, M.; El-Husseiny, A.; Radwan, A.E. A review on the applications of nuclear magnetic resonance (NMR) in the oil and gas industry: Laboratory and field-scale measurements. *J. Pet. Explor. Prod. Technol.* **2022**, *12*, 2747–2784. [[CrossRef](#)]
85. Lai, J.; Wang, G.; Wang, Z.; Chen, J.; Pang, X.; Wang, S.; Zhou, Z.; He, Z.; Qin, Z.; Fan, X. A review on pore structure characterization in tight sandstones. *Earth-Sci. Rev.* **2018**, *177*, 436–457. [[CrossRef](#)]
86. Timur, A. Nuclear magnetic resonance study of carbonate rocks. In *Proceedings of the SPWLA 13th Annual Logging Symposium*, Tulsa, OK, USA, 7–10 May 1972; OnePetro: Tulsa, OK, USA, 1972.
87. Chang, D.; Vinegar, H.J.; Morriss, C.; Straley, C. Effective porosity, producible fluid and permeability in carbonates from NMR logging. In *Proceedings of the SPWLA 35th Annual Logging Symposium*, Tulsa, OK, USA, 19–22 June 1994; OnePetro: Tulsa, OK, USA, 1994.

88. AlKharraa, H.S.; Wolf, K.-H.A.; Kwak, H.T.; Deshnenkov, I.S.; AlDuhailan, M.A.; Mahmoud, M.A.; Arifi, S.A.; AlQahtani, N.B.; AlQuraishi, A.A.; Zitha, P.L.J. A Characterization of Tight Sandstone: Effect of Clay Mineralogy on Pore-Framework. In Proceedings of the SPE Reservoir Characterisation and Simulation Conference and Exhibition, Abu Dhabi, United Arab Emirates, 24–26 January 2023; OnePetro: Tulsa, OK, USA, 2023.
89. Wang, R.; Shi, W.; Xie, X.; Zhang, W.; Qin, S.; Liu, K.; Busbey, A.B. Clay mineral content, type, and their effects on pore throat structure and reservoir properties: Insight from the Permian tight sandstones in the Hangjinqi area, north Ordos Basin, China. *Mar. Pet. Geol.* **2020**, *115*, 104281. [[CrossRef](#)]
90. Zou, C.; Zhu, R.; Liu, K.; Su, L.; Bai, B.; Zhang, X.; Yuan, X.; Wang, J. Tight gas sandstone reservoirs in China: Characteristics and recognition criteria. *J. Pet. Sci. Eng.* **2012**, *88–89*, 82–91. [[CrossRef](#)]
91. Yang, H.; Li, S.; Liu, X. Characteristics and resource prospects of tight oil and shale oil in Ordos Basin. *Acta Pet. Sin.* **2013**, *34*, 1.
92. Jia, A.; Wei, Y.; Guo, Z.; Wang, G.; Meng, D.; Huang, S. Development status and prospect of tight sandstone gas in China. *Nat. Gas Ind. B* **2022**, *9*, 467–476. [[CrossRef](#)]
93. Cook, J.E.; Goodwin, L.B.; Boutt, D.F. Systematic diagenetic changes in the grain-scale morphology and permeability of a quartz-cemented quartz arenite. *AAPG Bull.* **2011**, *95*, 1067–1088. [[CrossRef](#)]
94. Blunt, M.J.; Jackson, M.D.; Piri, M.; Valvatne, P.H. Detailed physics, predictive capabilities and macroscopic consequences for pore-network models of multiphase flow. *Adv. Water Resour.* **2002**, *25*, 1069–1089. [[CrossRef](#)]
95. Caineng, Z.; Zhang, G.; Zhi, Y.; Shizhen, T.; Lianhua, H.; Rukai, Z.; Xuanjun, Y.; Qiquan, R.; Denghua, L.; Zhiping, W. Concepts, characteristics, potential and technology of unconventional hydrocarbons: On unconventional petroleum geology. *Pet. Explor. Dev.* **2013**, *40*, 413–428.

Disclaimer/Publisher’s Note: The statements, opinions and data contained in all publications are solely those of the individual author(s) and contributor(s) and not of MDPI and/or the editor(s). MDPI and/or the editor(s) disclaim responsibility for any injury to people or property resulting from any ideas, methods, instructions or products referred to in the content.